Presented at the International Symposium on Heavy Vehicle Transport Technology (HVTT14)
Rotorua, New Zealand 2016

IMPROVING DIRECTIONAL STABILITY CONTROL IN A HEAVY TRUCK BY COMBINING BRAKING AND STEERING ACTION

M.Sc. in 2008 from Chalmers Uni. of Tech in Engineering Physic. Joined Volvo GTT in 2008 as a developer of motion control systems. Started as Ind. Phd student in 2012 being associated to Chalmers.

K. TAGESSON
Volvo Group Trucks Technology & Chalmers University of Technology, Sweden

Received a M.Sc. degree in Engineering Physics from Chalmers in 2003. He is currently a technical specialist at Sentient.

B. ERIKSSON
Sentient, Sweden

PhD degree in Machine and Vehicle Design, Chalmers, 1998. Currently CEO at Sentient - a vehicle motion control software product company.

J. HULTÉN
Sentient, Sweden

PhD degree from Linköping University in 2001. Between 2001 and 2009 he worked within vehicle industry and academia. Thereafter co-founder of Sentient where he currently is a technical specialist.

J. POHL
Sentient, Sweden

MSc. from Chalmers, 1996. Completed PhD within actuator coordination in 2007, Chalmers. Joined Volvo GTT in 2007, since 2013 Adj. Prof. at Chalmers, and since 2014 also Sr. tech. specialist.

L. LAINE
Volvo Group Trucks Technology & Chalmers University of Technology, Sweden

Ph.D. in vehicle propulsion, Chalmers in 1993. After 10 years in the automotive industry he became professor and group leader for the vehicle dynamics group at Chalmers where he currently acts.

B. JACOBSON
Chalmers University of Technology, Sweden

Abstract
The introduction of electronics in heavy vehicle steering systems has enabled active steering torque support. As steering is an effective way of escaping directional instability and brakes are fast and decoupled from the driver a combination of controlled steering and braking would be beneficial when performing directional stability control. A method is therefore proposed for this, based on control allocation. The method is unique in that it uses combined quadratic lateral and longitudinal tyre constraints computed in real-time, which has the potential of producing a higher corrective yaw moment than the commonly used approach with linear constraints, and that it can be adapted to any heavy vehicle combination. The method has been tested and compared to a standard stability control system in three different manoeuvres using a heavy solo tractor unit on a frozen lake. The measured deviation from the intended path was observed to reduce up to several meters with the new method. Also driver rating improved.
Keywords: Heavy Vehicles, Electronic Stability Control, Braking, Steering, Control Allocation

1 Introduction

Directional instability of heavy vehicles often leads to accidents. Based on data from US directional instability occurred in 9% of all accidents caused by a heavy vehicle from 2001 to 2003 (Kharrazi, 2012). This high rate of directional instability as a cause for accidents and a high rate of accidents caused by rollover together led to the introduction and later legislation of electronic stability control, ESC, in heavy trucks (European Union, 2011; NHTSA, 2012; UNECE, 2011). ESC is composed from two parts: (1) roll stability control; this is typically achieved by quickly reducing the speed of the vehicle combination. And (2) directional stability control, designed to support the driver when yaw stability is lost; this is typically achieved by reducing speed and applying selective individual wheel brake action. Rollover is most often the main stability problem for heavy vehicles under high friction conditions whereas directional instability is for low.

Based on accident data Høye (2011) estimates that ESC prevents about 40% of loss of control type accidents when fitted to a passenger car. Similar studies have not yet been performed for heavy trucks (Woodrooffe et al., 2009). Markkula et al. (2013) did however compare the benefit of a commercial ESC system in a truck driving simulator study run on a low friction road where a sudden lead vehicle braking scenario was used. A statistically significant reduction in loss of control was observed in repeated events when drivers were instructed to perform evasive steering. In these also the maximum body side slip angle observed was lower when ESC was turned on. In the initial unexpected runs, where drivers were left without instructions, the outcome was however slightly different. The subjects responded principally according to three different patterns: (1) only by braking and crashed, or (2) by initiating a gentle evasive steering manoeuvre early in time and managed to escape a crash, or (3) by initiating a large evasive steering manoeuvre late in time and crashed. Surprisingly, ESC activated (or would have if it had been on) in only 24% of the cases where a driver initiated a steering manoeuvre. This leaves a large number of subjects where ESC does not activate despite the efforts of the subjects to move the truck sideways. A simulation performed with the same vehicle model as used by Markkula et al. (2013) revels substantial understeer behaviour when applying a steering manoeuvre similar to that performed by these subjects. Understeer leads to low lateral vehicle response and thus also a higher risk of crash in the used scenario. There is thus room for improvement, at least in the understeer case.

The overall vehicle yaw moment that can be achieved by steering is in general higher than that of only selective individual wheel brake action. This is partly because the associated lever arms are longer for steering than for braking. However, a majority of heavy trucks produced are not equipped with steering actuators decoupled from the driver. Therefore effective yaw stabilisation considering only steering requires an accurate and immediate action by the driver. Markkula et al. (2014) validated various driver models against data taken from mentioned truck driving simulator study in (Markkula et al., 2013). It was found that the yaw rate nulling model agreed well with the steering action performed by drivers during vehicle yaw stabilisation on low friction. The model looks as follows

$$\dot{\delta}_H = -k \cdot \omega_z(t - \tau) \tag{1}$$

where $\dot{\delta}_H$ is the steering wheel angular rate, k a constant, ω_z vehicle yaw rate, t time, and τ a delay caused by reaction time. Found values of k for different drivers ranged from 11 s^{-1} to 24 s^{-1} and that of τ from 0.2 s to 0.45 s (for experienced drivers k ranged from 13 s^{-1} to 22 s^{-1} and τ from 0.22 s to 0.39 s). The variability in k together with high values of τ suggests that drivers are not in general capable of taking accurate immediate action when performing yaw

stabilisation. Yet the fact that steering is an effective way of achieving vehicle yaw stabilisation remains.

Electronic power steering, EPS, has been introduced recently on the truck market. This makes it possible to add extra steering wheel torque and thereby possibly change the steering wheel angular response of the driver. Some studies show that it is possible to change this response in a critical scenario by adding steering wheel torque, e.g. (Katzourakis, 2012), whereas others suggest the opposite, e.g. (Benderius, 2014). It seems likely that it could depend on the exact nature of the scenario. In the case of yaw stabilisation in a truck it has not been analysed. It is however clear that there will be limitations associated with steering wheel torque guidance for yaw stabilisation. This calls for a combination of steering torque guidance and brake action. A combination of braking and steering is also the most effective way to perform yaw stabilisation, as this will maximise the total vehicle yaw moment. This is also the focus of this paper — combined control of steering wheel torque and individual wheel brake action to achieve a more effective ESC system under low friction conditions. To achieve this a new control method is proposed and compared with an existing commercial system. The proposed method is developed to handle any vehicle combination, uses a new type of reference model, and strives for an optimal balance between braking and steering.

The structure of the paper is as follows: A top view of the control architecture followed by a detailed explanation of contained parts is presented in section 2; the setup of the performed ice track experiment is described in section 3; then the corresponding results together with a discussion follow in section 4; in the end conclusions are drawn in section 5. The proposed method can as said be configured to work for any vehicle combination but will for simplicity be described for a 4×2 tractor and semi-trailer combination in section 2. In the performed experiment, described in section 3 and 4, a solo 4×2 tractor unit was used (laden and unladen). The reason for not including a trailer in the experiments was limited carrying capacity of the ice. Further experiments including a trailer are however in scope of future plans. Notations used in the paper comply with ISO 8855 (ISO, 2011), with the exception that vector arrows are not being used. Units are SI unless otherwise stated.

2 Control Architecture and Design

The main structure of the proposed controller is shown in figure 1. The objective metric yaw rate of the truck unit has been chosen as a control objective. This is embodied in the reference yaw rate $\omega_{z,ref}$ serving as output from the Driver Interpreter block. It should here be pointed out that this metric could be exchanged for other properties, such as vehicle side-slip or lateral acceleration. The exact metric will not be in focus herein. The next block in figure 1 Stability Control is a proportional integrating, PI, controller with anti-windup generating a yaw moment request $\Delta M_{z,req}$ based on the reference yaw rate and a boolean signal, B_{sat}, indicating actuator saturation. The yaw moment request is fed into the Steering & Braking Coordination block that generates set-points for: EPS torque, T_{EPS}; for the individual truck wheel brake torque $T_{b,i}$ at wheel no. i ($\mathbf{T_b} = [T_{b,1}, T_{b,2}, ..., T_{b,N}]$); and for a longitudinal trailer coupling force $F_{trailer}$ (positive when the truck is being pulled backwards by the trailer). Some states are fed back from the vehicle this is illustrated with the state-vector $\mathbf{x}$. The content of the contained blocks in figure 1 will be deeper explained in the remainder of this section.

2.1 Driver Interpreter

A common approach taken when forming a reference vehicle objective is to use the steering wheel angle set by the driver and run this through an ideal vehicle model, which often forms

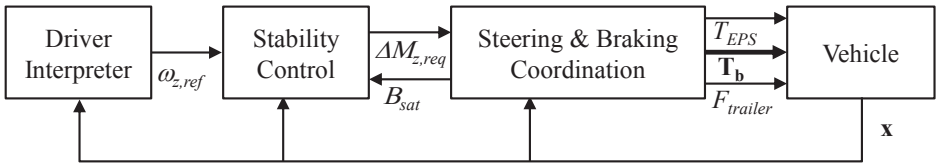

Figure 1 – Main structure of steering and braking controller

a first order lag (Manning & Crolla, 2007). By considering how a driver typically responds in an oversteer scenario, characterised in equation (1), it is clear that the driver is acting as a controller. Given that the road is straight the driver steers in order to make the yaw rate, ω_z, come to zero. This cannot be captured by only using information of the steering wheel angle. An observation about this was also made in (Markkula et al., 2015), where instead steering wheel angular velocity was used to determine a reference yaw rate that captures a target value of zero. The approach had however other shortcomings, making it less favourable, in other situations. The approach taken here is slightly different, but will still make $\omega_{z,ref} \approx 0$ in an oversteer scenario on a straight road. In a situation where the trajectory intended by the driver is not straight, for example in a double lane change, an ideal value of the reference would be $\omega_{z,ref} = v_x \kappa_R$. Where v_x is longitudinal vehicle speed and κ_R is instantaneous road curvature. Here it is assumed that the driver actually desires to follow the road. The details of the used Driver Interpreter block will not be presented in this paper for confidential reasons. Characteristic values of $\omega_{z,ref}$ produced within the experiments will however be shown in section 4 and compared with the ideal reference. The benefits of having a reference that better tracks the true desire of the driver are that: (1) the effectiveness of the ESC system to follow the desired road can be made independent of driver characteristics, (2) ESC activation dead-bands can be set tighter without risking nuisance, and (3) the driver can focus on steering the vehicle rather than steering the ESC system.

2.2 Stability Control

The translation from reference yaw rate $\omega_{z,ref}$ to yaw moment $\Delta M_{z,req}$ is made with a simple PI controller acting on the yaw rate error. Anti-windup is performed by using clamping. The proportional and integral control gains K_P and K_I are linearly speed dependent.

2.3 Steering & Braking Coordination

The mapping performed from vehicle yaw moment to actuator inputs is done in two intermediate steps. First force allocation is performed where lateral and longitudinal forces are computed. These forces are thereafter converted in a second step to the actuator format T_{EPS}, $\mathbf{T_b}$ and $F_{trailer}$.

Force Allocation

Control allocation is commonly used for over-actuated systems, meaning that there are more actuators than controlled motions (Johansen & Fossen, 2013). In this application there is only one controlled global force, that is the yaw moment, but there are several brake actuators and one steering actuator. There might consequently exist multiple solutions. With control allocation a solution is made unique by introducing a secondary objective; for instance the minimization of the actuator vector l^2-norm. By further using weighting matrices and relevant actuator constraints it is possible to control the characteristics of the unique solution. Schofield et al. (2006) proposed the usage of quadratic constrains to represent friction ellipses in a control allocation problem, but did however approximate these as linear constrains in the final implementation. Knobel et al. (2006) presented a non-linear method where friction ellipses are represented.

Real-time performance was however not shown. Tondel & Johansen (2005) produced solutions offline to a non-linear allocation problem, including a detailed tyre model. These solutions were thereafter stored and used in real-time. The main difference of the implementation used here to previous implementations is the introduction of quadratic constrains in order to represent friction ellipses, while the problem is solved in real-time. The usage of quadratic friction constrains enables a slightly higher resulting yaw moment made up of both steering and braking forces, compared to what is possible with a linear approximation. It also removes the conflict that appears between braking and steering with linear constraints as the maximum yaw moment is sought. The full formulation of the quadratic allocation problem used is

$$\begin{aligned} u = \arg\min(&\|W_u(u-u_d)\|_2^2 + \gamma\|(Bu-v)\|_2^2) \\ &\text{subject to } u_{min} \leq u \leq u_{max} \\ &\quad \& \ \frac{1}{2}u^\intercal H_1 u + d_1 \leq 0 \quad \& \ \frac{1}{2}u^\intercal H_2 u + d_2 \leq 0 \quad \& \ \frac{1}{2}u^\intercal H_3 u + d_3 \leq 0 \end{aligned} \tag{2}$$

where u is a vector with elements that correspond to specific actuator forces, W_u is a weighting matrix, u_d is a desired set-point for u, γ is a scalar weight usually set high to emphasise the importance of the term $\|(Bu-v)\|_2^2$, B is the effectiveness matrix that maps the actuator vector u to a resulting global force, and v is the desired global force. The desired global force here is $\Delta M_{z,req}$, but as a trick to capture friction constraints accurately a nominal vehicle yaw moment is added according to $v = \Delta M_{z,req} + aF_{yf0}$, where a is the distance from centre of gravity, c.o.g., to the front axle, and F_{yf0} is the lateral force acting on the front axle in the absence of actuator involvement. The yaw moment contribution from aF_{yf0} is removed in a later step. Concerning the constraints listed, u_{min} and u_{max} are lower and upper actuator constraints respectively. The three matrices H_1, H_2, and H_3 together with the three vectors d_1, d_2, and d_3 constitute the three quadratic constraints that represent the friction ellipses on the front axle of the tractor, rear axle of the tractor, and trailer respectively. As there is no actuator on the rear axle of the tractor nor on the considered trailer working in the lateral direction the second and third quadratic constraints can be simplified to linear ones. The one on the front axle will however remain. The problem presented in equation (2) is known as a quadratically constrained quadratic program, QCQP, (Boyd & Vandenberghe, 2004). Given that the matrices $W_u^\intercal W_u + \gamma B^\intercal B$, H_1, H_2, and H_3 are all positive semi-definite then the problem is convex and a unique solution exist if the feasible region is non-empty (Palomar & Eldar, 2010).

For the targeted combination the actuator vector is set as $u = [F_{yf1}, F_{yf2}, F_{xf}, F_{xr}, F_{trailer}]^\intercal$. To start with, steering is only considered on the front axle. In the force allocation step this is represented as a lateral tyre force F_{yf}. As it can be desirable to activate only steering and not braking for small yaw moment requests the force F_{yf} is further split into two parts F_{yf1} and F_{yf2}, satisfying $F_{yf1} + F_{yf2} = F_{yf}$. By having low penalty on F_{yf1} set by W_u this element will be prioritised up to a suitable limit specified by corresponding elements in u_{min} and u_{max}. Next, as a pair of brakes on the same axle is considered to never activate simultaneously during an ESC intervention it is possible to reduce the allocation problem size by collapsing two variables into one according to $F_{xfl} = \max(F_{xf}, 0)$ and $F_{xfr} = \max(-F_{xf}, 0)$, where F_{xfl} is the front left longitudinal force, F_{xfr} is the front right longitudinal force, and F_{xf} represents a longitudinal force that can act both forwards and backwards. The element F_{xr} is defined analogously for the rear axle. A lateral force will also act on the rear axle, denoted F_{yr0}, in the absence of actuator involvement. This will have an effect upon possible values of F_{xr}. It is therefore included in the term d_2. Finally, $F_{trailer}$ is as previously introduced the total trailer braking force acting on the truck. The desired actuator vector is set as $u_d = [0, F_{yf0}, 0, 0, 0]^\intercal$, where the second entry forces the allocated forces to be symmetric in a vicinity of the nominal lateral force F_{yf0}. The

effectiveness matrix used is $B = [a, a, b_f/2, b_r/2, -e \sin \Delta\Psi_n]$, where b_f and b_r are track width front and rear respectively, e is the distance from the centre of gravity of the tractor unit to the coupling point, and $\Delta\Psi_n$ is the yaw articulation angle between the tractor and the trailer. An example of patterns formed by the allocator is shown in Appendix I, figure 6.

Conversion to Actuator Format
In the longitudinal direction a conversion is made to brake pressure simply by assuming a linear relation between pressure and longitudinal force, thus assuming that no other torque is acting on the same wheel and that small steering angles apply[1]. For instance on the front left wheel the brake pressure is set as $P_{b,1} = k_b \cdot \max(F_{xf}, 0)$.

The guiding steering wheel torque T_{EPS} is determined by computing a zero shift wheel angle as

$$\delta_{f,ZERO} = (F_{yf} - F_{yf0})/C_{\alpha f} \tag{3}$$

where $C_{\alpha f}$ is the cornering stiffness of the front axle. This angle is used to move the steering characteristics of the EPS system so that zero steering wheel torque corresponds to this angle.

The brake pressure of a trailer should be controlled so that a force $F_{trailer}$ is acting in the fifth wheel coupling. This will not discussed in more detail in here.

3 Experiment Setup

The proposed control method was implemented and tested in a 4×2 tractor unit on a frozen lake in northern Sweden. This section will provide details about the test vehicle, how the controller was implemented, and what test manoeuvres that were used.

3.1 Test Vehicle & Instrumentation

Used test vehicle was a solo Volvo FH 4×2 tractor unit having: a wheelbase of 3.7 m, a 13 litre engine, unladen weight of 6050 kg on front axle and 2380 kg on rear axle, laden weight of 8440 kg on front axle and 11022 kg on rear axle, and a steering gear ratio of 18.6. A Geidobler swap body for tractor units was filled with blocks of iron and fitted when laden tests were run. The tractor was equipped with a high precision dual-antenna RTK GPS system; providing position, speed, and orientation information at 10 Hz. In addition also standard on-board sensors were used.

The standard ESC system fitted to the truck was used as a reference (hereafter denoted 'ESC^0') and turned off when running the new proposed controller (hereafter denoted 'ESC$^+$'). Brake pressure requests from ESC$^+$ were sent directly to the ABS modulators at 100 Hz (constrained by brake ECU sample rate). The anti-lock braking system, ABS, was always turned on and consequently set a lower brake pressure than what was requested in the event of excessive wheel brake slip. The truck was further equipped with an EPS system providing an interface to request an angle $\delta_{f,ZERO}$ at 1100 Hz (constrained by ESC$^+$ base sampling time), when this was done the normal steering characteristics also became stiffer than normal. When running ESC^0 standard production steering torque support was provided.

[1] In the tests performed this assumption was consistent. In a future implementation a more general solution would be preferred.

3.2 Controller Implementation

ESC$^+$ (described in section 2) was implemented on a dSpace Autobox II. The QCQP problem (in equation (2)) was solved with the tool Forces Pro (Domahidi & Jerez, 2014). The sample rate of the controller was 900 μs (1100 Hz). This was selected short enough to provide stable steering torque feedback, without oscillations, and long enough to be able to execute the algorithms. As no trailer was included the force allocation formulation differed from that described in section 2 in that the last element of u, u_d, and B as well as the last constrain in equation (2) was removed. The first quadratic constrain in equation (2) was set as

$$\frac{1}{2}u^\intercal \underbrace{\begin{bmatrix} 2 & 2 & 0 & 0 \\ 2 & 2+\frac{8}{1000} & 0 & 0 \\ 0 & 0 & 8 & 0 \\ 0 & 0 & 0 & 0 \end{bmatrix}}_{=H_1} u \leq \underbrace{(\mu F_{zf})^2}_{=-d_1} \tag{4}$$

where μ is friction level. This was set manually based on straight brake test recordings in the trials, but can typically be estimated quickly in the types of manoeuvres intended for ESC (Andersson et al., 2007). Including a friction estimator is suggested for future work. The term F_{zf} is vertical front axle load. Furthermore, the term $\frac{8}{1000}$ was introduced as a numerical trick to make the matrix H_1 strictly positive definite, which was required by be solver (Domahidi & Jerez, 2014). The second quadratic constrain in equation (2) did as mentioned earlier turn into a linear constrain and was therefore merged with the existing linear constrain according to

$$\underbrace{[-\Delta F_{yf1}, -\infty, -\infty, -\frac{1}{2}\sqrt{(\mu F_{zr})^2 - F_{yr0}^2}]}_{=u_{min}} \leq u \leq \underbrace{[\Delta F_{yf1}, \infty, \infty, \frac{1}{2}\sqrt{(\mu F_{zr})^2 - F_{yr0}^2}]}_{=u_{max}} \tag{5}$$

where ΔF_{yf1} is a range parameter for F_{yf1} (interval where only steering is commanded) that was tuned to get a very low level of nuisance brake action during normal driving. The last element of u (that is F_{xr}) is limited by available friction after first considering the already acting lateral force, F_{yr0}. The lateral forces acting on the front tyre group F_{yf0} and the rear tyre group F_{yf0} were estimated from side slip estimates at the corresponding axles and a linear tyre model with friction saturation. Side slips were estimated from GPS speed and heading signals (10Hz). Onboard yaw rate and lateral acceleration sensors were used to interpolate this data to 100Hz. The only parameters used in the tyre model was saturation limits, $\pm\mu F_{zf}$ front and $\pm\mu F_{zr}$ rear, axle cornering stiffness front, $C_{\alpha f}$, and axle cornering stiffness rear, $C_{\alpha r}$. Parameter values used in the experiment are listed in Appendix, table 1 .

3.3 Test Cases

Three test manoeuvres where run: double lane change (laden and unladen), high speed entering curve (laden), and brake pulse rear in curve (laden and unladen). An illustration of the manoeuvres is provided in figure 2. In all the entry speed was determined by running with ESC deactivated and increasing the entry speed in steps of 5 km/h until it was no longer possible to follow the intended course within reasonable limits. This value was used as entry speed in the test. The first manoeuvre double lane change, DLC, was chosen to excite both understeer and oversteer behaviour. The second, high speed entering curve, HSC, was chosen to excite pure understeer. And last, brake pulse rear in curve, BPC, was chosen to excite pure oversteer by applying a heavy brake pulse on the rear axle, subjectively tuned right before test run (Unladen: amplitude 3 bar, duration 1 s; laden: amplitude 8 bar, duration 1.5 s). The dimensions of the manoeuvres were mainly chosen as a consequence of available space.

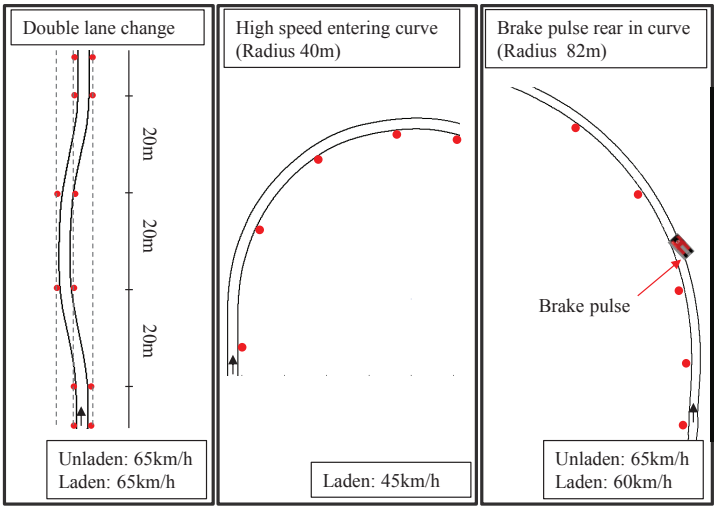

Figure 2 – Illustration of the three test cases used

A test driver was instructed to maintain the intended entry speed until right before the manoeuvre started where neutral gear was selected; thereafter try to perform as precise steering as possible to maintain the intended course with released brake pedal. The intended course was marked with cones. As a complement to objective measures the test driver reported a subjective grade after every run between 1 and 10 describing how hard the course was to complete. The scale was defined so that 0 represented impossible and 10 easy for anyone. Runs with ESC$^+$ and standard ESC was completed at least three times per manoeuvre and loading condition. As the ice was polished by the scrubbing wheels it was noted that the course became more slippery for every run. To get a fair comparison between systems switching was therefore made between the two after every run.

4 Results and Discussion

Both objective and subjective results from ESC$^+$ and ESC^0 will be presented and discussed in this section, one test case at the time. Runs are presented as consecutive pairs as ice conditions quickly changed. In the objective comparison the following metrics are considered: (1) Representing the level of risk of a run the maximum deviation from intended course Δy_{max} (most distant point of the truck to intended course). (2) Driver activity as steering wheel angle δ_H and steering wheel torque M_H. (3) Controller activity as measured brake pressure P_B (commanded brake pressure, but limited by ABS). (4) And vehicle motion as instantaneous curvature $1/R$ (yaw rate divided by speed) and body side slip β at c.o.g.

4.1 Double Lane Change

Objective results from DLC runs, can be seen in figure 3. All plots have travelled distance s on the x-axis. The colours red is always used for ESC^0 runs and blue for ESC$^+$ runs. The maximum deviation from the intended course is kept below 1 m in all runs within the first part of the manoeuvre. In the later part (s >60 m i.e. when going back to original lane) the deviation is much lower in ESC$^+$ runs than in ESC^0. Driver steering wheel angular response also seems similar in the two cases up until s >60 m where a clear separation occurs as a cause of the course deviation (most prominent in laden case). The steering wheel torque is very different in the two cases. This is mostly due to the difference in steering wheel torque characteristics. Furthermore as the front axle saturates the ESC$^+$ controller tries to limit the amount of excessive steering that the driver is applying by suggesting a more optimal level. When the driver exceeds this

level a counteracting steering wheel torque will appear. This can for instance be seen in the first unladen ESC$^+$ run at around 65 m of travel. Whether this feature had an effect upon the driver in the DLC runs is not clear. The driver did however comment about the apparent difference.

In figure 3 the plots that are showing brake pressure have dashed lines to represent brake pressure front (maximum of front left and front right) and solid lines to show brake pressure rear (maximum of rear left and rear right). As seen the applied brake pressure differs a lot between ESC^0 and ESC$^+$. In the unladen case ESC$^+$ uses small brake pulses often primarily on the front axle, and in some cases also short ones on the rear axle. ESC^0 only pushes rather heavy brake action on the front axle at some rare events. In the laden case the same pattern can be seen but the brake pulses commanded by ESC^0 sometimes reach very high. As ESC$^+$ control is striving for an optimal balance between braking and steering no heavy braking is seen, since this would have reduced lateral steering forces in large parts of the manoeuvre. The plots that are showing instantaneous curvature include a solid blue and red line showing the actual values (ω_z/v_x), thick dashed lines showing the corresponding reference used ($\omega_{z,ref}/v_x$), and a solid black line showing ω_z/v_x from a reference run performed at low speed in the same course. The reference taken from ESC$^+$ is tracking the reference run a lot better than the ESC^0 is doing. This is one of the reasons of why earlier brake action can be applied by ESC$^+$ than by ESC^0 in the case of instability, as it is able to track that ultimately desired by the driver also in the normal case; which is to follow the road. Finally, in the last row of plots in figure 3 the body side slip reviles clear side slip instability in the later part of the manoeuvre when running ESC^0 laden. In the unladen case the high lateral deviation performed by ESC^0 appears to be due to an understeer nature possibly caused by excessive front axle braking.

The driver gave a subjective grades of the runs shown in figure 3 as follows: ESC$^+$ unladen [6.5,6.5,6.5]; ESC^0 unladen [6.5,5,5]; ESC$^+$ laden [7.5,6.5,5]; ESC^0 laden [3,3,3].

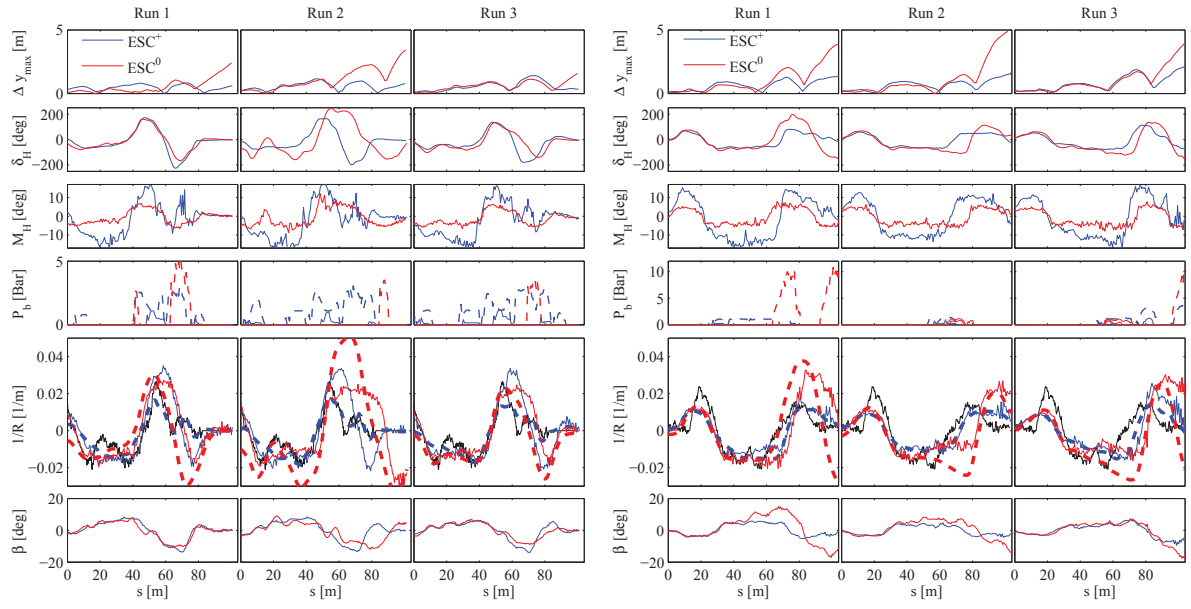

(a) Unladen (b) Laden

Figure 3 – Double lane change

4.2 High Speed Entering Curve

Results for HSC are shown in figure 4. Lines included are analogous to those in figure 3 apart from that here a circular shape is used therefore the optimal instantaneous curvature is simply the inverse of the radius, which is not as noisy as that attained from a low speed reference run. Starting with the maximum deviation from the intended course it is seen in figure 4 that again ESC$^+$ performs better than ESC^0. Both show substantial deviation, $\sim$5 m, but with ESC$^+$ the vehicle comes back to the intended course after a while. The underlying reason is a small yaw moment created by rear axle brake action and also brake action on the front inner wheel. Even though the front axle is saturated by lateral forces ESC$^+$ tries to find an even bigger yawing moment by also introducing mild brake action. Eventually this causes speed to go down more than in the ESC^0 case, making it possible to get back to the intended course. When looking at the underlying curvature references being used it is clear that neither of the two behaves well. Excessive steering is causing this phenomenon in the case of ESC^0 and a known point for improvement for ESC$^+$. The behaviour would however not change in this scenario for ESC$^+$, if the reference would track the true course better, as both the PI controller and the allocator are saturated and would do so also for an improved version of the reference. Also here ESC$^+$ is trying to guide the driver to follow the optimal steering wheel angle to follow the course. This is why high steering wheel torque is seen. No major difference in used steering wheel angle can however be seen. In this scenario the driver chose not to grade the runs as the observed maximum deviation from the intended course was an obvious indicator of performance.

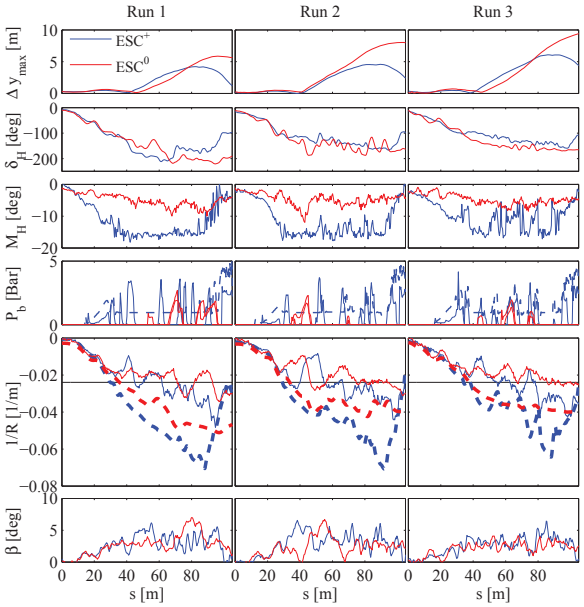

Figure 4 – High speed entering curve (laden)

4.3 Brake Pulse Rear in Curve

Figure 5 shows results from the BPC case (analogous lines to figure 4). The brake pulse ends at $s = 0$ m and leaves the vehicle with a high body side slip. The curvature reference of ESC$^+$ is now clearly tracking that defined by the circle a lot better than ESC^0. Furthermore, another clear difference that can be observed is that ESC$^+$ is working at higher side slip angles while at the same time maintaining a slightly lower path deviation, whereas ESC^0 is clearly penalising high body side slip at the expense of higher path deviation, by applying heavy brake action on the

front axle. In other words understeer is considered more safe than oversteer or that 'oversteer minimization' has highest priority.

The driver gave a subjective grades of the runs shown in figure 3 as follows: ESC^+ unladen [5,7.5,6]; ESC^0 unladen [4,5.5,4]; ESC^+ laden [6,5,2]; ESC^0 laden [1,3,1]. As the driver is seated in the front of the vehicle which is tracking the course better in the ESC^+ case than in the ESC^0 case this might be a reason for higher grades. It is hard for the driver to estimate where the rear part of the vehicle is in relation to the course. This might serve as an explanation to the discrepancy between subjective rating and maximum path deviation.

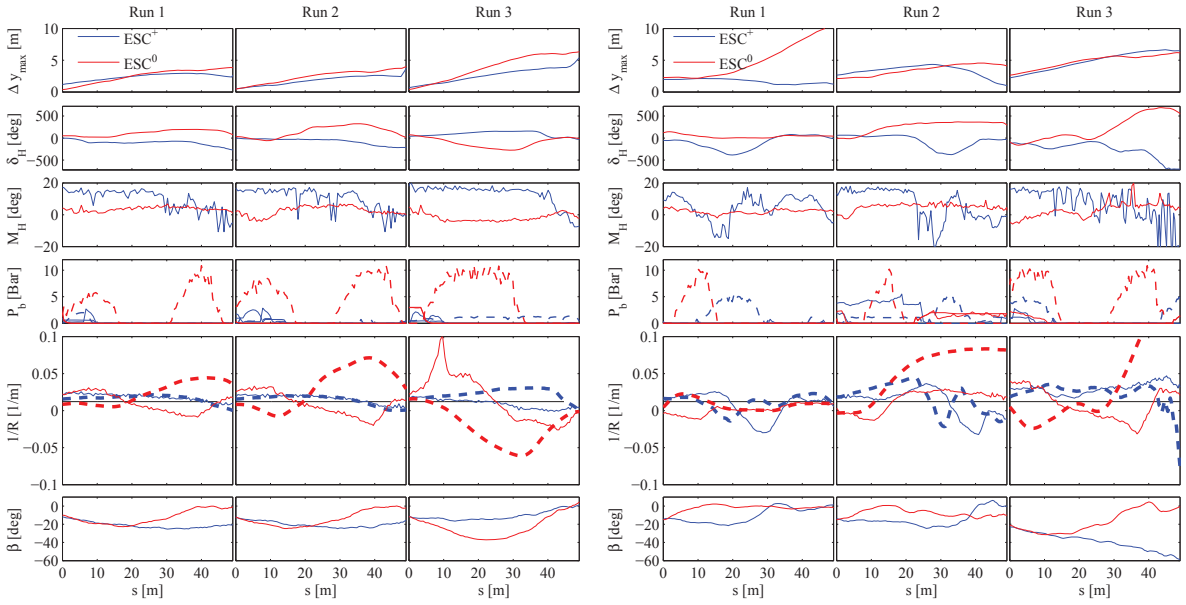

(a) Unladen (b) Laden

Figure 5 – Brake pulse rear in curve

5 Conclusion

Drivers are not very accurate when performing steering corrections during yaw stabilisation. A method has been proposed to combine both steering wheel torque and brake action for a truck combination. As the method is considering combined lateral and longitudinal tyre force constrains it has the potential to achieve more effective stabilisation than when the two are kept separate. This was also verified in an experiment with a 4×2 solo tractor unit on a frozen lake where three different manoeuvres where run and where a standard ESC system was used as reference. The observed deviation from the path was lowered in all the three manoeuvres by a few centimetres up to several meters, depending on the manoeuvre, with the proposed method. Also driver rating improved when introducing the new method. The results further shows that with a well behaving reference model and good balance between braking and steering forces it is possible to avoid 'oversteer minimization' and instead perform better path tracking. Recall that only 24% of all drivers managed to trigger ESC in a realistic avoidance scenario, where the front axle saturated in (Markkula et al., 2013) even though many crashed into a leading vehicle. Future work should include testing with one or several trailing units, as well as a variety of drivers in order to better understand the benefits and limitations. Also integration with normal braking is important, as well as roll over prevention. The used control objective yaw rate should also possibly be extended.

References

Andersson, M., Bruzelius, F., Casselgren, J., Gäfvert, M., Hjort, M., Hultén, J., Håbring, F., Klomp, M., Olsson, G., Sjödahl, M. et al. (2007), 'Road friction estimation', *Saab Automobile AB, Trollhättan, Sweden*.

Benderius, O. (2014), Modelling driver steering and neuromuscular behaviour, PhD thesis, Chalmers University of Technology.

Boyd, S. & Vandenberghe, L. (2004), *Convex optimization*, Cambridge university press.

Domahidi, A. & Jerez, J. (2014), 'FORCES Professional', embotech GmbH (`http://embotech.com/FORCES-Pro`).

European Union (2011), 'REGULATION (EC) No 661/2009'.

Høye, A. (2011), 'The effects of electronic stability control (esc) on crashes, an update', *Accident Analysis & Prevention* **43**(3), 1148–1159.

ISO (2011), Road vehicles – vehicle dynamics and road-holding ability – vocabulary, Technical Report ISO 8855:2011, International Organization for Standardization.

Johansen, T. & Fossen, T. (2013), 'Control allocation a survey', *Automatica* **49**(5), 1087–1103.

Katzourakis, D. (2012), Driver steering support interfaces near the vehicles handling limits, PhD thesis, Tu Delft.

Kharrazi, S. (2012), Steering based lateral performance control of long heavy vehicle combinations, PhD thesis, Chalmers University of Technology.

Knobel, C., Pruckner, A. & Bünte, T. (2006), 'Optimized force allocation: A general approach to control and to investigate the motion of over-actuated vehicles', *IFAC Proceedings Volumes* **39**(16), 366–371.

Manning, W. & Crolla, D. (2007), 'A review of yaw rate and sideslip controllers for passenger vehicles', *Transactions of the Institute of Measurement and Control* **29**(2), 117–135.

Markkula, G., Benderius, O. & Wahde, M. (2014), 'Comparing and validating models of driver steering behaviour in collision avoidance and vehicle stabilisation', *Vehicle System Dynamics* **52**(12), 1658–1680.

Markkula, G., Benderius, O., Wolff, K. & Wahde, M. (2013), 'Effects of experience and electronic stability control on low friction collision avoidance in a truck driving simulator', *Accident Analysis & Prevention* **50**, 1266–1277.

Markkula, G., Eklov, J., Laine, L., Wikenhed, E. & Frojd, N. (2015), Improving yaw stability control in severe instabilities by means of a validated model of driver steering, *in* 'Intelligent Vehicles Symposium (IV), 2015 IEEE', IEEE, pp. 18–23.

NHTSA (2012), '49 CFR Part 571, Docket No. NHTSA-2015-0056: Federal Motor Vehicle Safety Standards; Electronic Stability Control Systems for Heavy Vehicles'.

Palomar, D. P. & Eldar, Y. C. (2010), *Convex optimization in signal processing and communications*, Cambridge university press.

Schofield, B., Hagglund, T. & Rantzer, A. (2006), Vehicle dynamics control and controller allocation for rollover prevention, *in* '2006 IEEE Conference on Computer Aided Control System Design, 2006 IEEE International Conference on Control Applications, 2006 IEEE International Symposium on Intelligent Control', IEEE, pp. 149–154.

Tondel, P. & Johansen, T. (2005), Control allocation for yaw stabilization in automotive vehicles using multiparametric nonlinear programming, *in* 'Proceedings of the American Control Conference', Vol. 1, Citeseer, p. 453.

UNECE (2011), 'Addendum 12: Regulation No. 13, Revision 7'.

Woodrooffe, J., Blower, D., Gordon, T., Green, P. E., Liu, B. & Sweatman, P. (2009), Safety benefits of stability control systems for tractor-semitrailers, Technical Report DOT HS 811 205, NHTSA.

Appendix I: Allocation Characteristics

The allocator distributes forces as illustrated in figure 6. Different nominal lateral force levels F_{yf0} and F_{yr0} are marked with green circles. Blue plus marks represent solutions for varying values of $\Delta M_{z,req}$. The flat pattern on both sides of F_{yf0} in the left subplot is built up from increasing values of F_{yf1}. Further away the solutions start to travel in a direction where lateral and longitudinal forces are combined. The slope of these branches of solutions can easily be changed with the elements in W_u. In the right subfigure it can be observed how the allowed longitudinal force is affected by the nominal lateral axle force F_{yr0}.

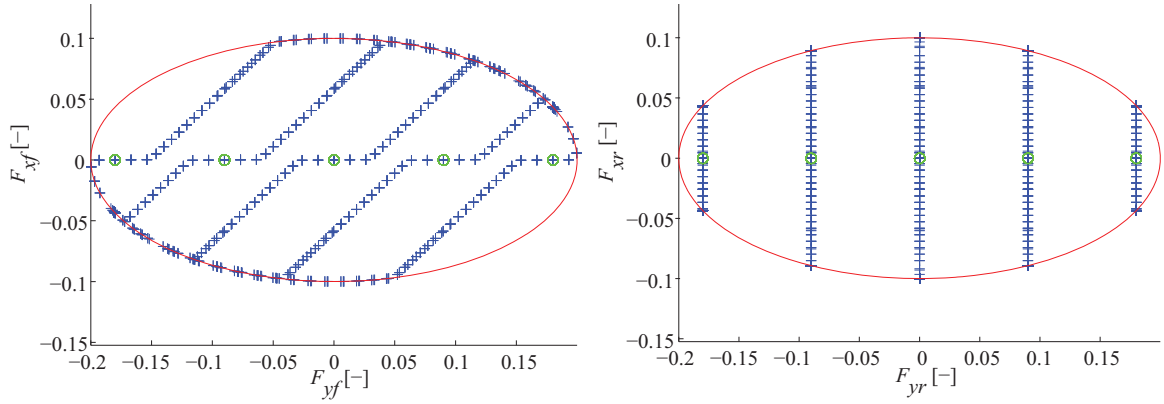

Figure 6 – Example of allocated forces after being normalized (divided with the normal force of the axle.) The friction coefficient is set to 0.2 and $\alpha = 0$, hence $F_{trailer} = 0$.

Appendix II: Parameter Values

Table 1 – Values of parameters used in experiment

Property	Value	Unit	Description
K_P	1000	Nm/(m·rad/s^2)	Proportional gain
K_I	50000	Nm/(m·rad/s)	Integral gain
W_u	diag([0.1,1.0,0.5,1.59])	-	Weighting matrix (unladen)^2
	diag([0.1,1.0,0.5,0.88])	-	Weighting matrix (laden)
γ	100	-	Scalar weight
a	1.05	m	Distance c.o.g. to front axle (unladen)
	2.10	m	Distance c.o.g. to front axle (laden)
b_f	2.05	m	Track width front
b_r	1.85	m	Track width rear
μ	0.4	-	Friction coefficient
F_{zf}	59411	N	Vertical front axle load (unladen)
	82881	N	Vertical front axle load (laden)
F_{zr}	23372	N	Vertical rear axle load (unladen)
	108240	N	Vertical rear axle load (laden)
ΔF_{yf1}	4500	N	Only steering limit
$C_{\alpha f}$	297	kN/rad	Front cornering stiffness (unladen)
	414	kN/rad	Front cornering stiffness (laden)
$C_{\alpha r}$	117	kN/rad	Rear cornering stiffness (unladen)
	541	kN/rad	Rear cornering stiffness (laden)
k_b	2.3×10^{-7}	Bar/N	Brake factor